Structure of the E.coli signal recognition particle bound to a translating ribosome

Schaffitzel, C.; Oswald, M.; Berger, I.; Ishikawa, T.; Abrahams, J.P.; Koerten, H.K.; ... ; Ban, N.

LETTERS

Structure of the *E. coli* signal recognition particle bound to a translating ribosome

Christiane Schaffitzel[1], Miro Oswald[1], Imre Berger[1], Takashi Ishikawa[1], Jan Pieter Abrahams[2], Henk K. Koerten[3], Roman I. Koning[3] & Nenad Ban[1]

The prokaryotic signal recognition particle (SRP) targets membrane proteins into the inner membrane[1–4]. It binds translating ribosomes and screens the emerging nascent chain for a hydrophobic signal sequence, such as the transmembrane helix of inner membrane proteins. If such a sequence emerges, the SRP binds tightly, allowing the SRP receptor to lock on. This assembly delivers the ribosome-nascent chain complex to the protein translocation machinery in the membrane. Using cryo-electron microscopy and single-particle reconstruction, we obtained a 16 Å structure of the *Escherichia coli* SRP in complex with a translating *E. coli* ribosome containing a nascent chain with a transmembrane helix anchor. We also obtained structural information on the SRP bound to an empty *E. coli* ribosome. The latter might share characteristics with a scanning SRP complex, whereas the former represents the next step: the targeting complex ready for receptor binding. High-resolution structures of the bacterial ribosome and of the bacterial SRP components are available, and their fitting explains our electron microscopic density. The structures reveal the regions that are involved in complex formation, provide insight into the conformation of the SRP on the ribosome and indicate the conformational changes that accompany high-affinity SRP binding to ribosome nascent chain complexes upon recognition of the signal sequence.

The targeting of membrane proteins by SRPs is universal for all kingdoms of life[1–4], and eukaryotic SRPs (which contain a 300-nucleotide RNA and six proteins[5]) also target presecretory proteins to the endoplasmatic reticulum. Prokaryotic SRPs are smaller; the *E. coli* SRP consists of a 4.5S RNA (Ffs) and a single 48-kDa protein (Ffh, fifty-four homologue). The Ffh protein has three domains, termed N, G and M. The N and G domains are structurally and functionally coupled[1]. Ribosome binding is mediated through the N domain[6,7], which has a four-helix bundle. The G domain has a Ras-like GTPase fold with an additional insertion box motif that is unique to SRP GTPases. The methionine-rich M domain contains the hydrophobic signal sequence binding pocket and binds Ffs[1,3,8]. Both Ffs and Ffh are conserved and are essential for viability, and hence they represent a minimal functional version of the complex. A cryo-electron microscopy (EM) structure of a eukaryotic SRP–ribosome complex is available[9], but at present there are no structures of prokaryotic SRP–ribosome complexes.

Stable *E. coli* ribosomal nascent chain complexes (RNCs) were generated by *in vitro* translation[10]. The nascent chain contained the transmembrane helix (TMH) of *E. coli* FtsQ, which had been previously observed to cross-link to Ffh[11]. After *in vitro* translation, the RNCs were purified by sucrose gradient centrifugation and affinity chromatography (Supplementary Fig. 1). The SRP bound strongly even to non-translating ribosomes under physiological salt conditions. Only under high-salt conditions could a significantly higher affinity of SRPs to RNCs than to empty ribosomes be detected (Supplementary Fig. 1). Under the conditions chosen for the EM experiments, virtually all RNCs were in complex with SRPs, which is consistent with observed dissociation constants (∼0.1 nM for the RNCs and 50–90 nM for 70S ribosomes)[6,12,13]. The three-dimensional cryo-EM reconstruction of the RNC–SRP complex has a resolution of 16 Å (Fourier shell correlation (FSC) 0.5, see Supplementary Fig. 1; 11 Å according to the 3σ criterion), whereas that of the 70S–SRP complex is about 20 Å (see Supplementary Table 1).

In the RNC, all three active sites of the ribosome are occupied by transfer RNAs. However, the occupancy at the A-site is significantly lower than at the fully occupied P- and E-sites, so the nascent chain is connected mostly to P-site tRNA. The SRP is positioned at the polypeptide tunnel exit, as expected. The RNA part of the SRP can be recognized in the density by its helical appearance. The SRP adopts an elongated shape (170 Å × 75 Å) that projects away from the polypeptide tunnel exit (Fig. 1). The polypeptide tunnel exit is not covered by the SRP, and the nascent chain is still accessible to other factors. This is a marked difference from the eukaryotic SRP, which covers the polypeptide tunnel exit[9]. Another important difference in *E. coli* SRP is the absence of the Alu domain, which in eukaryotes stalls translation by interfering with elongation-factor binding[9].
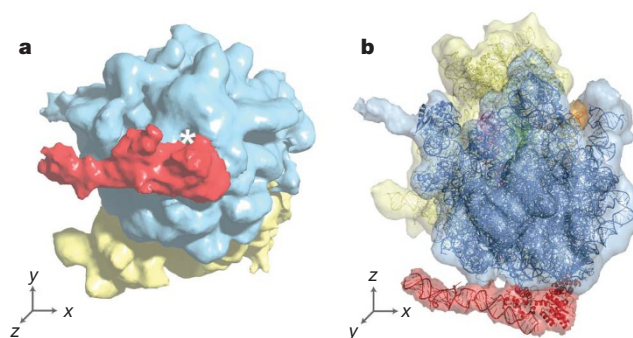

Figure 1 | Cryo-EM structure of the RNC–SRP complex. Ribosomal subunits are shown in yellow (30S) and blue (50S). The SRP is shown in red and is displayed at a lower contour level than the RNC complex. The RNC–SRP complex is shown with the view into the polypeptide exit tunnel (white star) (**a**) and from the back of the 50S subunit (**b**). A-, P- and E-site tRNAs are coloured magenta, green and orange, respectively. The crystal structures of 70S, tRNAs and a molecular model of SRP have been fitted into the density.

[1]ETH Zurich, Institute for Molecular Biology and Biophysics, HPK Building, Schafmattstrasse 20, 8093 Zurich, Switzerland. [2]Department of Biophysical Structural Chemistry, Leiden Institute of Chemistry, Gorlaeus Laboratories, Leiden University, 2300 RA Leiden, The Netherlands. [3]Leiden University Medical Center, Molecular Cell Biology, Center for Electron Microscopy, PO Box 9600, 2300 RC Leiden, The Netherlands.

The coordinates of the *E. coli* 70S ribosome crystal structure[14] were fitted into the density using SITUS[15]. The SRP was modelled as two rigid bodies from two sources: the NG domain of *Thermus aquaticus* in complex with the non-hydrolysable GTP analogue GMPPNP[16]; and the M domain in complex with RNA domain IV from *Sulfolobus solfataricus*[17]. Finally, the remainder of the 4.5S RNA was built as an extension of domain IV using a model from the SRP database[18]. The density revealed a bipartite structure for 4.5S RNA with two mostly straight helical regions of around 55 Å and 77 Å in length, and a pronounced kink of approximately 130° at the joint (Fig. 2). After manual readjusting, the SRP model was further improved using normal mode flexible fitting[19] and energy minimization with CNS software[20].

Independent fitting of the NG and M domains in complex with the 4.5S RNA resulted in an SRP conformation that is different from the crystal structure of the archaeal SRP core[17]. Our data indicated a 180° rotation about a flexible hinge region at the carboxyl terminus of the G domain in addition to a 130° rotation along the axis of the linker helix between the NG and M domains of Ffh (Fig. 2c). These flexible regions stretch upon binding and position the M domain almost 20 Å away from the NG domain—resulting in a more elongated, less compact shape of bound as compared to unbound SRP. The crystal structure of the archaeal SRP core has been suggested to present a closed, compact conformation of the SRP, which could exist in the non-ribosome bound state and could rearrange and open up upon ribosome binding[21].

We identified four distinct contact sites (c1–c4) between the SRP and the large ribosomal subunit (Fig. 3a), but in the absence of a signal peptide in the RNC, only the c1 contact remains (see Supplementary Fig. 3). In the first contact site (c1), the N domain of Ffh mainly contacts ribosomal protein L23, and to a far lesser degree L29 (Fig. 3a, b). This is in agreement with previous crosslinking experiments[6,22]. C1 is conserved in the eukaryotic structure[9], where flexible loops of the N domain contact L23 and L29, so that the

domain is positioned almost perpendicular to the surface of the ribosome (see Supplementary Fig. 4). In our structure, by contrast, the N domain contacts L23 with its helices and the G domain is in the vicinity of L29. Consequently, the relative positioning of the NG and M domains is different (see Supplementary Information).

The contact area between Ffh and L23/L29 is formed mainly by three helices (h1–h3) of the N domain. It features a patch of positively charged residues at the binding interface (see Supplementary Fig. 2) juxtaposed to the negatively charged residues on the surface of L23, which could explain the salt-sensitivity of the 70S–SRP complex (see Supplementary Fig. 1c). The G domain of Ffh is positioned above L29 and could also contribute to ribosome binding. In contrast to eukaryotic SRP[7], we did not find crosslinks between the *E. coli* SRP and L29, perhaps because residues17 and 25 used in the crosslinking studies are positioned at the tip of the N domain four-helix bundle and point away from L29 in our structure[6,12].

Strikingly, L23 is also the main contact point of two other factors that interact with nascent chains: the translocon and the ribosome-associated chaperone trigger factor (TF). At the last stage of co-translational protein targeting, the translocon, SecYEG, replaces the SRP and their binding is mutually exclusive. Consequently, we observe that the SRP and SecYEG[10] use almost identical contact areas (c1, c2 and c4) for their interactions with the ribosome. On the other hand, biochemical evidence exists showing that the SRP and TF can bind simultaneously to the ribosome[12,13] and compete for the nascent chain[23]. In our structure, the contact between the SRP and L23, which is mediated by the N domain of the SRP, does not seem to overlap with the anchor point of TF, which interacts with a relatively small surface area of the ribosome using a flexible loop (see Supplementary Information)[24]. However, an SRP bound to the translating ribosome as visualized in this study would sterically hinder access of TF to its ribosomal binding site. Therefore, an additional conformational change in SRP would be necessary to explain simultaneous binding of TF and SRP to the ribosome. It is possible that this is the reason for
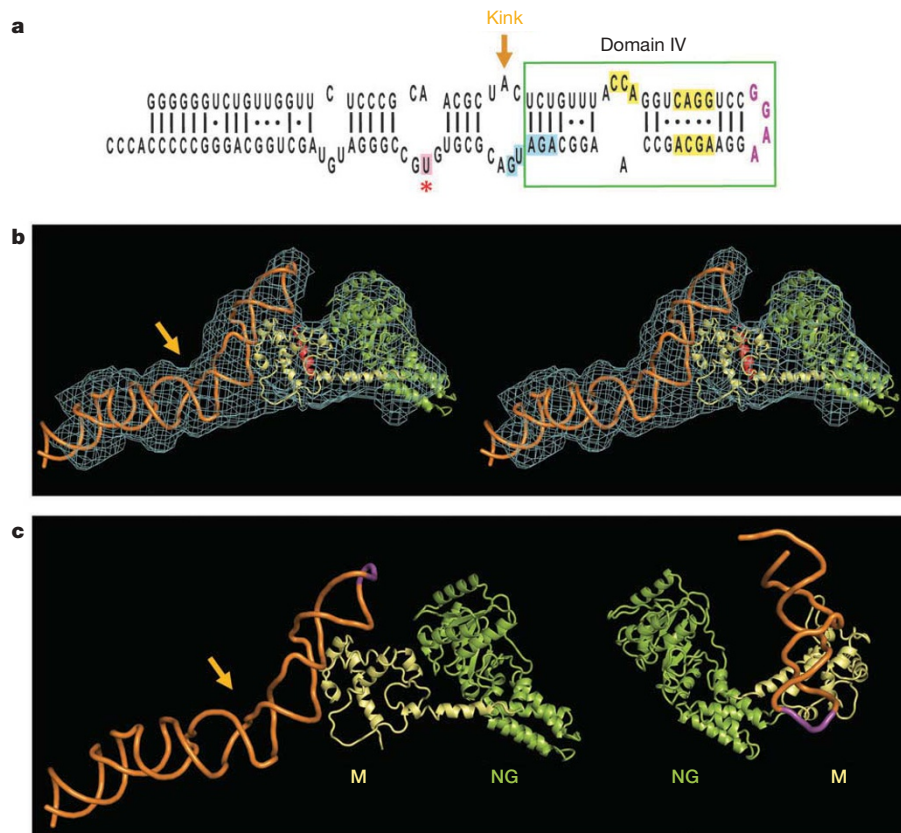

Figure 2 | Molecular model of the SRP bound to a translating ribosome. a, Secondary structure of SRP RNA with the M-domain binding site (yellow), ribosome contact region (blue), tetra-loop (magenta) and crosslink site U84 (red star). The conserved domain IV is marked with a green box. **b,** Stereo view of the molecular model of *E. coli* SRP. Density is shown in cyan, 4.5S RNA in orange, Ffh M domain in yellow, Ffh NG domain in green and the TMH in red. **c,** Comparison between the molecular model of *E. coli* SRP (left) and the crystal structure of SRP54 and SRP RNA domain IV[17] (right). For orientation, the RNA tetra-loop is shown in magenta. The kink region is marked by an orange arrow.
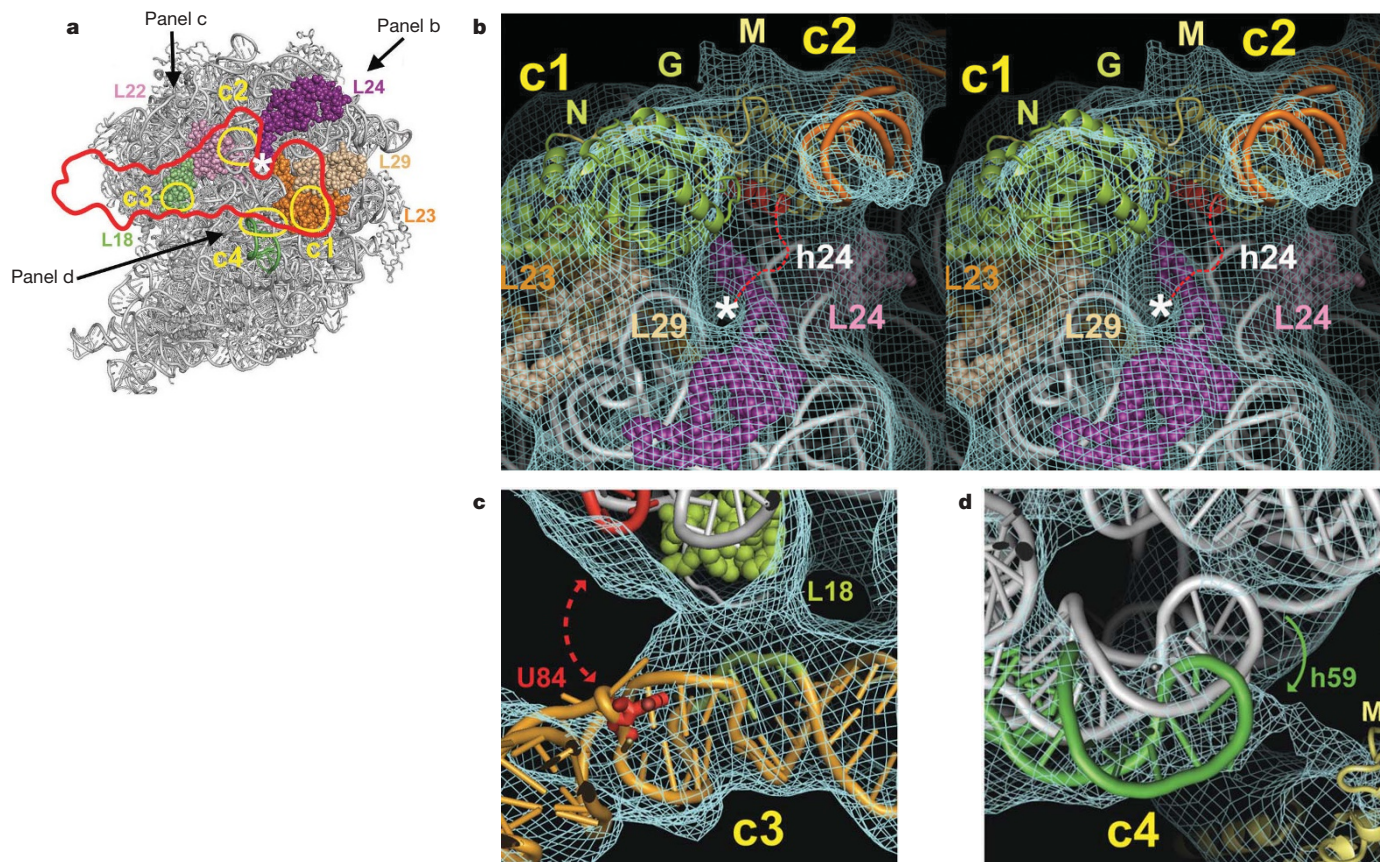
Figure 3 | Contact sites of SRP on 50S. a, Overview. SRP is outlined in red and the four contacts in yellow on the crystal structure of 70S. **b**, Stereo view of the ribosomal tunnel exit (white star). A model of the nascent chain with TMH anchor is shown in red. **c**, Contact 3. Nucleotides 72–76 of 4.5S RNA and L18 are shown in green, and the crosslink site U84 and nucleotides 2,828–2,837 of 23S RNA are shown in red[25]. **d**, Contact 4 and conformational changes in helix 59. 23S RNA as observed in the crystal structure[14] is shown in grey, helix 59 conformation in the RNC–SRP complex in green, and the Ffh M domain in yellow. The density is displayed at high contour level ($\sigma = 2.5$).

the 25% reduction in affinity of SRP for a TF–ribosome complex[13], and the decrease in crosslinking efficiency between SRP position 17 and L23 in the presence of TF[12].

The second SRP–ribosome contact (c2) is mediated mainly by helix 24 of 23S RNA and to a lesser extent by proteins L24 and L22. On the SRP side, the contact is formed by the C-terminal helix M5 of the M domain and could also involve the linker between helices M3 and M4. Helix M5 is probably also involved in the binding of the signal anchor[8].

The third contact site (c3) is furthest from the polypeptide tunnel exit. It involves ribosomal protein L18 and 4.5S RNA, probably nucleotides 72–76. These residues are part of domain IV and of the kink region of 4.5S RNA (Fig. 2a). C3 is adjacent to nucleotides 2,828–2,837 of 23S RNA, to which U84 of 4.5S RNA has been cross-linked in the presence of a nascent chain[25] (Fig. 3c).

In the fourth contact site (c4), we observed a pronounced (9 Å) movement of helix 59 of 23S RNA towards the SRP M domain (Fig. 3d). This rather large conformational change indicates that the ribosome is not a rigid platform for SRP binding. However, it is not clear whether it might serve to communicate the state of the ribosome to other factors.

The M domain of SRP has a hydrophobic groove, which was suggested to be part of the signal anchor-binding site of the nascent chain[8,17]. Our structure shows that this groove is very close to the exit of the ribosomal tunnel (Fig. 3b). According to this model, the TMH is buried between the M domain and the ribosome. Conversely, in the absence of the signal sequence, the SRP may only contact the ribosome at protein L23 via its N domain, which has been characterized as the ribosome-binding domain of SRP[6,22] (Fig. 4). This is in agreement with our reconstruction of a 70S–SRP complex without a

nascent chain, in which SRP density was only present at c1 (see Supplementary Fig. 3). This interaction would allow the M domain to scan the nascent peptide for a signal sequence in a translating ribosome, which results in full SRP docking at c2–c4 upon recognition of a signal sequence, as visualized in the SRP–RNC reconstruction.
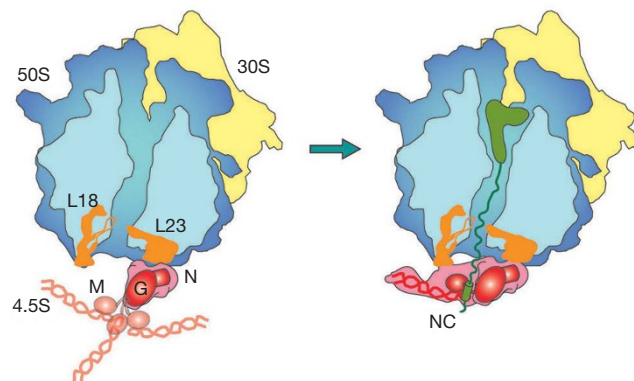

Figure 4 | Model of signal anchor-dependent docking of SRP to the ribosome. In the absence of a nascent chain, the SRP binds via its N domain to L23, and the M domain scans for a nascent chain with a signal anchor. In this state, the M domain with Ffs is flexible. Upon recognition of a signal anchor, the SRP binds tightly to the ribosome and forms three additional contacts with 50S. The signal anchor is buried in the hydrophobic pocket of the M domain, and the NG domain has an increased affinity for GTP, which is a prerequisite for FtsY binding[2,30]. 30S, yellow; 50S, blue; peptidyl-tRNA, green; SRP, red; contact proteins, orange.

This is further supported by the RNA–RNA crosslink next to c3 (Fig. 3c), which is seen only in the presence of a nascent chain with a signal sequence[25]. The formation of additional contacts coupled with the interactions between the hydrophobic signal sequence and the M domain of Ffh would explain salt-resistant binding of the SRP to the translating ribosome with picomolar affinity (Fig. 4).

We have previously determined the cryo-EM structure of the *E. coli* RNC–translocon complex at 15 Å resolution[10]. Together, these two structures set the stage for further structural studies aimed at deciphering at the molecular level the entire process of co-translational targeting and translocation in prokaryotes.

METHODS

SRP–RNC complexes were generated and characterized as described in the Supplementary Information. For grid preparation, RNCs (100 nM final concentration) were incubated on ice for 30 min with a 19-fold molar excess of SRP in 50 mM HEPES-KOH pH 7.5, 100 mM KCl, 25 mM MgCl$_2$, 1 mM DTT and 1 mM GTP. Micrographs were recorded at a magnification of ×50,000 under low-dose conditions with an FEI Tecnai F20 electron microscope operated at 200 kV. Micrographs were scanned on a Nikon super coolscan 9000 scanner, corresponding to a pixel size of 1.27 Å on the object scale. Subsequently, the data were 3× binned to 3.81 Å per pixel. 63,000 RNC particles were picked manually using X3d, CTF-corrected by CTF-Mix[26], and analysed with the SPIDER software package[27]. Supervised classification[28] computationally separated empty ribosomes from SRP-bound ribosomes. 27,400 particles (43.5%) had the same Euler angles for the alignment against the empty ribosome and the SRP-bound ribosome and a better correlation coefficient for the SRP-bound ribosome (see also Supplementary Information). The final resolution was assessed by Fourier shell correlation characteristics: ~11 Å at 3σ and ~16 Å at FSC 0.5 (See Supplementary Fig. 1 and Supplementary Table 1). The map was low-pass filtered to 11 Å (the 3σ resolution). The X-ray structure of 70S (main body, L7/12 and L1 stalk)[14] was fitted as rigid bodies using the program SITUS version 2.2[15]. Helix 59 was readjusted manually using O[29]. The *T. aquaticus* Ffh NG domain[16], the *S. solfataricus* M domain with RNA[17], and the remainder of the 4.5S RNA[18] were placed manually using O[29]. The long flexible linker of *S. solfataricus*[17] was rebuilt using O. The fit of SRP was further refined using NOMAD for normal mode flexible fitting[19] (see Supplementary Information) and was energy-minimized using CNS Version 1.1[20].

1. Keenan, R. J., Freymann, D. M., Stroud, R. M. & Walter, P. The signal recognition particle. *Annu. Rev. Biochem.* **70**, 755–775 (2001).
2. Nagai, K. *et al.* Structure, function and evolution of the signal recognition particle. *EMBO J.* **22**, 3479–3485 (2003).
3. Doudna, J. A. & Batey, R. T. Structural insights into the signal recognition particle. *Annu. Rev. Biochem.* **73**, 539–557 (2004).
4. Ulbrandt, N. D., Newitt, J. A. & Bernstein, H. D. The *E. coli* signal recognition particle is required for the insertion of a subset of inner membrane proteins. *Cell* **88**, 187–196 (1997).
5. Walter, P. & Blobel, G. Signal recognition particle contains a 7S RNA essential for protein translocation across the endoplasmic reticulum. *Nature* **299**, 691–698 (1982).
6. Gu, S. Q., Peske, F., Wieden, H. J., Rodnina, M. V. & Wintermeyer, W. The signal recognition particle binds to protein L23 at the peptide exit of the *Escherichia coli* ribosome. *RNA* **9**, 566–573 (2003).
7. Pool, M. R., Stumm, J., Fulga, T. A., Sinning, I. & Dobberstein, B. Distinct modes of signal recognition particle interaction with the ribosome. *Science* **297**, 1345–1348 (2002).
8. Keenan, R. J., Freymann, D. M., Walter, P. & Stroud, R. M. Crystal structure of the signal sequence binding subunit of the signal recognition particle. *Cell* **94**, 181–191 (1998).
9. Halic, M. *et al.* Structure of the signal recognition particle interacting with the elongation-arrested ribosome. *Nature* **427**, 808–814 (2004).
10. Mitra, K. *et al.* Structure of the *E. coli* protein-conducting channel bound to a translating ribosome. *Nature* **438**, 318–324 (2005).
11. Valent, Q. A. *et al.* Nascent membrane and presecretory proteins synthesized in *Escherichia coli* associate with signal recognition particle and trigger factor. *Mol. Microbiol.* **25**, 53–64 (1997).
12. Buskiewicz, I. *et al.* Trigger factor binds to ribosome-signal-recognition particle (SRP) complexes and is excluded by binding of the SRP receptor. *Proc. Natl Acad. Sci. USA* **101**, 7902–7906 (2004).
13. Raine, A., Ivanova, N., Wikberg, J. E. & Ehrenberg, M. Simultaneous binding of trigger factor and signal recognition particle to the *E. coli* ribosome. *Biochimie* **86**, 495–500 (2004).
14. Schuwirth, B. S. *et al.* Structures of the bacterial ribosome at 3.5 Å resolution. *Science* **310**, 827–834 (2005).
15. Wriggers, W., Milligan, R. A. & McCammon, J. A. Situs: A package for docking crystal structures into low-resolution maps from electron microscopy. *J. Struct. Biol.* **125**, 185–195 (1999).
16. Padmanabhan, S. & Freymann, D. M. The conformation of bound GMPPNP suggests a mechanism for gating the active site of the SRP GTPase. *Structure* **9**, 859–867 (2001).
17. Rosendal, K. R., Wild, K., Montoya, G. & Sinning, I. Crystal structure of the complete core of archaeal signal recognition particle and implications for interdomain communication. *Proc. Natl Acad. Sci. USA* **100**, 14701–14706 (2003).
18. Rosenblad, M. A., Gorodkin, J., Knudsen, B., Zwieb, C. & Samuelsson, T. SRPDB: Signal Recognition Particle Database. *Nucleic Acids Res.* **31**, 363–364 (2003).
19. Lindahl, E., Azuara, C., Koehl, P. & Delarue, M. NOMAD-Ref: visualization, deformation and refinement of macromolecular structures based on all-atom normal mode analysis. *Nucleic Acids Res.* **34**, W52–W56 (2006).
20. Brünger, A. T. *et al.* Crystallography & NMR system: A new software suite for macromolecular structure determination. *Acta Crystallogr.* **D54**, 905–921 (1998).
21. Wild, K., Halic, M., Sinning, I. & Beckmann, R. SRP meets the ribosome. *Nature Struct. Mol. Biol.* **11**, 1049–1053 (2004).
22. Ullers, R. S. *et al.* Interplay of signal recognition particle and trigger factor at L23 near the nascent chain exit site on the *Escherichia coli* ribosome. *J. Cell Biol.* **161**, 679–684 (2003).
23. Eisner, G., Moser, M., Schäfer, U., Beck, K. & Müller, M. Alternate recruitment of signal recognition particle and trigger factor to the signal sequence of a growing nascent polypeptide. *J. Biol. Chem.* **281**, 7172–7179 (2006).
24. Ferbitz, L. *et al.* Trigger factor in complex with the ribosome forms a molecular cradle for nascent proteins. *Nature* **431**, 590–596 (2004).
25. Rinke-Appel, J. *et al.* Crosslinking of 4.5S RNA to the *Escherichia coli* ribosome in the presence or absence of the protein Ffh. *RNA* **8**, 612–625 (2002).
26. Conway, J. F. & Steven, A. C. Methods for reconstructing density maps of "single" particles from cryoelectron micrographs to subnanometer resolution. *J. Struct. Biol.* **128**, 106–118 (1999).
27. Frank, J. *et al.* SPIDER and WEB: processing and visualization of images in 3D electron microscopy and related fields. *J. Struct. Biol.* **116**, 190–199 (1996).
28. Valle, M. *et al.* Cryo-EM reveals an active role for aminoacyl-tRNA in the accommodation process. *EMBO J.* **21**, 3557–3567 (2002).
29. Jones, T. A., Zou, J. Y., Cowan, S. W. & Kjeldgaard, M. Improved methods for building protein models in electron density maps and the location of errors in these models. *Acta Crystallogr. A* **47**, 110–119 (1991).
30. Bacher, G., Lütcke, H., Jungnickel, B., Rapoport, T. A. & Dobberstein, B. Regulation by the ribosome of the GTPase of the signal-recognition particle during protein targeting. *Nature* **381**, 248–251 (1996).

CORRIGENDUM

A positive-feedback-based bistable 'memory module' that governs a cell fate decision

Wen Xiong & James E. Ferrell Jr

In Box 1, equation (1) should read

$$\frac{\mathrm{d}[A^*]}{\mathrm{d}t} = \{\text{stimulus} \times ([A_{\text{tot}}] - [A^*])\} + f\frac{[A^*]^n}{K^n + [A^*]^n}([A_{\text{tot}}] - [A^*]) - k_{\text{inact}}[A^*]$$

Setting $\frac{\mathrm{d}[A^*]}{\mathrm{d}t} = 0$, it follows that stimulus $= \dfrac{f \times [A^*]^n[A_{\text{tot}}] - k_{\text{inact}}K^n[A^*] - (f + k_{\text{inact}})[A^*]^{n+1}}{([A^*] - [A_{\text{tot}}])([A^*]^n + K^n)}$

which implicitly defines all of the possible steady state values of $[A^*]$ for any given value of the stimulus. The plots in Box 1 show only the stable steady states (the sections of the curves with positive slopes).

ERRATUM

RNA-templated DNA repair

Francesca Storici, Katarzyna Bebenek, Thomas A. Kunkel,
Dmitry A. Gordenin & Michael A. Resnick

In Figure 1, the column header indicating the repair frequencies should read "Repair frequency $(\text{Leu}^+) \times 10^{-7}$" rather than "Repair frequency $(\text{Leu}^+) \times 10^{-3}$ (per 10^7 viable cells)".

CORRIGENDUM

Structure of the *E. coli* signal recognition particle bound to a translating ribosome

Christiane Schaffitzel, Miro Oswald, Imre Berger, Takashi Ishikawa,
Jan Pieter Abrahams, Henk K. Koerten, Roman I. Koning & Nenad Ban

During the preparation of the manuscript, we inadvertently mislabelled ribosomal protein L32 as ribosomal protein L18 when interpreting the density based on the 50S coordinates (PDB accession number 2AW4). Therefore, whenever L18 is mentioned in the text and in Figs 3 and 4, it should be considered to refer to ribosomal protein L32. Our results and conclusions are not affected.